Joint experimental and computational study of silicon dioxide electron energy loss spectra

Massimiliano Filippi,[1] Lucia Calliari,[1] and Maurizio Dapor[1,2]
[1]*ITC-irst, via Sommarive 18, I-38050 Povo, Trento, Italy*
[2]*Dipartimento di Fisica dell' Università di Trento, I-38050 Povo, Trento, Italy*
(Received 28 November 2006; revised manuscript received 11 January 2007; published 7 March 2007)

Experimental reflection electron energy loss spectra from silicon dioxide are excited by electrons with energy ranging from 90 eV to 2 keV. A Monte Carlo simulation, shortly described, is utilized to calculate the same spectra. The comparison between simulated and experimental spectra shows substantial agreement, particularly at high exciting energies. Differences at low exciting energies are mainly ascribed to surface effects.

DOI: 10.1103/PhysRevB.75.125406 PACS number(s): 79.20.Uv, 72.20.Dp

I. INTRODUCTION

In a previous paper,[1] a Monte Carlo simulation of the energy loss spectrum of electrons backscattered by silicon dioxide was presented and discussed. Though the resulting spectra could be understood in terms of the SiO_2 band structure, a comparison with experimental electron energy loss (EEL) spectra was missing in that case.

In this paper, we present a joint experimental and theoretical investigation of the SiO_2 EEL spectrum. A range of exciting energies, from 90 eV to 2 keV, is considered, and this provides the opportunity to single out surface and bulk contributions to the EEL spectrum. We show that Monte Carlo (MC) simulated spectra, based on an energy loss function (ELF) derived from optical data, agree fairly well with experimental spectra excited by energies around 2 keV. However, when the exciting energy decreases, the agreement worsens. This is ascribed to the fact that surface effects do set in.

II. EXPERIMENT

X-ray photoemission spectra (XPS), Auger electron spectra (AES), and reflection electron energy loss spectra (REELS) are measured with a PHI545 instrument equipped with a double-pass cylindrical mirror analyzer, a coaxial electron gun, and a nonmonochromatic x-ray source ($h\nu = 1253.6$ eV).

SiO_2 was in the form of a 36 nm thick amorphous film on Si. It was annealed at 800 °C in ultrahigh vacuum before inserting into the analysis chamber (base pressure of 2×10^{-10} mbar). XPS wide scans revealed less than 1% C contamination. A Si (100) N-doped sample was cleaned in the analysis chamber by 4 keV Ar^+ sputtering. No C contamination was revealed by AES wide scans.

EEL spectra were excited by primary electrons (impinging at an angle of 30° from the surface normal) with energy E_0 ranging from 90 eV to 2 keV. They were acquired at a constant energy resolution of 0.6 eV, as measured on the Pd Fermi edge of a He *I* ($h\nu$=21.2 eV) excited valence-band photoemission spectrum. Once acquired, spectra were corrected for the energy dependence ($E^{0.9}$) of the analyzer transmission function. To keep electron-induced damage to a minimum, the current density was lower than 40 A/m^2 and the acquisition time was less than 6 min. For each acquisition, the electron beam was moved to a new sample position. A diagram of the experimental configuration is given in Fig. 1.

III. MONTE CARLO SIMULATION

Many details of the Monte Carlo code utilized in this context can be found in Refs. 1 and 2. As a consequence, we will limit ourselves to summarize the method used.

The step length Δs is given by

$$\Delta s = -\lambda \ln(\mu_1), \tag{1}$$

where μ_1 is a random number uniformly distributed in the range (0, 1) and λ is the electron mean free path:

$$\lambda(E) = \frac{1}{N[\sigma_{inel}(E) + \sigma_{el}(E)]}. \tag{2}$$

Here $\sigma_{inel}(E)$ and $\sigma_{el}(E)$ are the inelastic and elastic scattering cross sections, respectively, while N is the number of SiO_2 molecules per unit volume in the target.

Before each collision, a random number μ_2 uniformly distributed in the range (0, 1) is generated and compared with the probability of inelastic scattering q_{inel}. The probability of inelastic scattering is given by

$$q_{inel} = \frac{\sigma_{inel}}{\sigma_{inel} + \sigma_{el}}, \tag{3}$$

while, of course, that of elastic scattering is $q_{el}=1-q_{inel}$. If the random number μ_2 is less than or equal to the probability of inelastic scattering, then the collision will be inelastic; otherwise, it will be elastic.

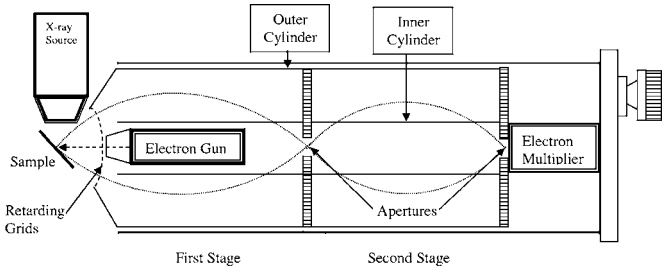

FIG. 1. Diagram of the experimental configuration.

If the collision is elastic, the polar scattering angle θ is selected so that the probability $P_{el}(\theta,E)$ of elastic scattering into an angular range from 0 to θ is a random number μ_3 uniformly distributed in the range (0, 1):

$$\mu_3 = P_{el}(\theta,E) = \frac{1}{\sigma_{el}} \int_0^{\theta} 2\pi \sin\vartheta \frac{d\sigma_{el}}{d\Omega} d\vartheta. \quad (4)$$

Note that σ_{el} is obtained by integrating the function $2\pi \sin\vartheta\, d\sigma_{el}/d\Omega$ from 0 to π rad.

If the collision is inelastic, the energy loss W is computed by utilizing a random number μ_4 uniformly distributed in the range (0, 1), so that the probability $P_{inel}(W,E)$ providing the fraction of electrons losing energies less than or equal to W is given by

$$\mu_4 = P_{inel}(W,E) = \frac{1}{\sigma_{inel}} \int_0^{W} \frac{d\sigma_{inel}}{dw} dw. \quad (5)$$

Note that σ_{inel} is obtained by integrating the differential inelastic scattering cross sections $d\sigma_{inel}/dw$ from 0 to $W_{max} = E/2$ to take into account the fact that a scattered projectile electron cannot be distinguished from a target electron.

For inelastic scattering collisions, the polar scattering angle θ is calculated by using the classical binary-collision model, which is sufficiently accurate for many practical purposes:

$$\frac{W}{E} = \sin^2\theta. \quad (6)$$

The azimuthal angle, for both elastic and inelastic collisions, is calculated as a random number uniformly distributed in the range $(0, 2\pi)$.

The particles are followed in their trajectories until their energies become lower than $(E_0 - 60)$ eV or until they leave the solid target.

The number of trajectories for each backscattered electron energy distribution calculation is of the order of 10^8.

The differential elastic-scattering cross section needed to compute the probability $P_{el}(\theta,E)$ has been calculated by using the well-known relativistic partial wave expansion method; for an excellent review see Ref. 3. Details of the present calculation and comparison with many experimental data can be found in Refs. 2 and 4.

To calculate the probability $P_{inel}(W,E)$, the differential inelastic-scattering cross section has been obtained by using Ashley's approximated extension of the ELF to momentum transfer greater than zero:[5]

$$\frac{d\sigma_{inel}(w,E)}{dw} = \frac{me^2}{2\pi\hbar^2 NE} \mathrm{Im}\left[\frac{-1}{\varepsilon(0,w)}\right] \left\{ \left[1 - \left(\frac{w}{E}\right)\right] \ln\frac{4E}{w} - \frac{7}{4}\left(\frac{w}{E}\right) + \left(\frac{w}{E}\right)^{3/2} - \frac{33}{32}\left(\frac{w}{E}\right)^2 \right\}, \quad (7)$$

where m is the electron mass, e is the electron charge, and $\hbar$ is the Planck constant divided by 2π. The optical data $\varepsilon(0,w)$ for the present Monte Carlo code were obtained from the atomic scattering factors by Henke *et al.*[6] and, for energies lower than 40 eV, the Buechner experimental ELF, $\mathrm{Im}\left[\frac{-1}{\varepsilon(0,w)}\right]$, was utilized.[7]

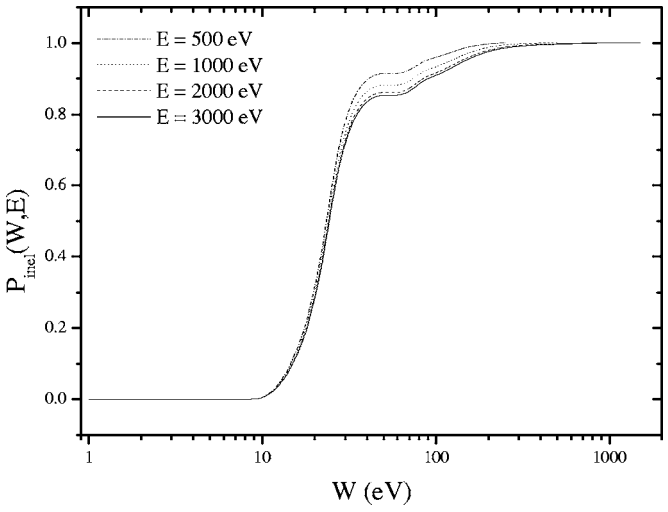

FIG. 2. SiO_2 distribution function $P_{inel}(W,E)$ [Eq. (5)] for inelastic collisions of electrons in SiO_2 causing energy losses less than or equal to W. The distribution is represented as a function of the energy loss W for four values of the incident electron kinetic energy E.

In order to assure very accurate numerical integrations of the inelastic-scattering cross section used to calculate the inelastic-scattering probabilities and inelastic mean free paths, we used a cubic spline interpolation to compute the values of the optical ELF between experimental points. All the numerical integrations were performed by Bode's rule. The distribution function $P_{inel}(W,E)$ for inelastic collisions of electrons in SiO_2 causing energy losses less than or equal to W, as computed by numerically integrating the differential inelastic-scattering cross section by Bode's rule [using Eq. (5)], is presented in Fig. 2. Similar trends have been reported for Si by Bichsel.[8] The distributions for SiO_2 are presented here as a function of the energy loss W for four values of the incident electron kinetic energy E (500, 1000, 2000, and 3000 eV). Functions such as these, calculated for several energies E, are stored in a file from which the Monte Carlo code can extract the value of the energy loss W at every inelastic collision.

Proceeding in a similar way, *mutatis mutandis*, one obtains the scattering angle at every elastic collision.

IV. RESULTS AND DISCUSSION

MC simulated (continuous line) and experimental (dotted line) EEL spectra are compared in Fig. 3 for two different primary electron energies (2 keV and 500 eV). Spectra are normalized to a common area (counts eV) of the zero loss peak, so that the resulting intensity is given in eV^{-1}. Loss energies up to 60 eV are considered. Simulated and experimental spectra both reproduce the basic loss features, namely, the plasmon peaks corresponding to single ($\approx$23 eV) and double ($\approx$46 eV) excitations. On the other hand, differences between the two spectra are found in the

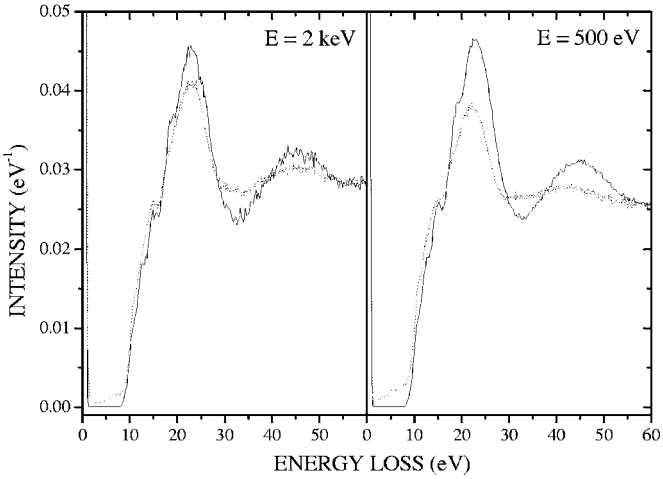

FIG. 3. Experimental (dotted line) and MC simulated (solid line) EEL spectra excited by 2 keV (left) and 500 eV (right) electrons. All spectra are normalized to a common area of the zero loss peak. The resulting intensity is thus given in eV^{-1}.

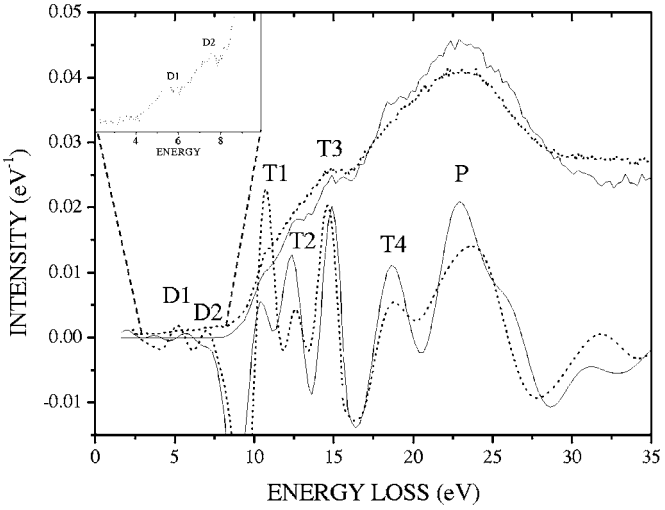

FIG. 4. Experimental (dotted line) and MC simulated (solid line) EEL spectra excited by 2 keV electrons. The two spectra are normalized to a common area of the zero loss peak. The negative second derivative of each spectrum (experimental, dotted line; MC, continuous line) is provided, on an arbitrary intensity scale, as a means to resolve spectral contributions. The band-gap region for the experimental spectrum is enlarged in the inset.

gap region (below ≈10 eV) and in the feature intensity. As for the former, MC simulated spectra show the zero loss intensity expected for an ideal wide gap material, whereas experimental spectra show nonzero loss intensity, thereby revealing the existence of defect-related states within the gap for the real material. As for the overall loss intensity, we see that simulated spectra are always more intense than experimental spectra. The difference in intensity increases as the primary energy decreases. At 500 eV, we observe also an energy shift in the peak maximum between the experimental and MC simulated spectra. It is thus clear that simulated spectra, based on a loss function derived from optical data, best agree with experimental spectra excited by high-energy electrons.

A more detailed comparison between the MC simulated (continuous line) and experimental (dotted line) spectra is presented in Fig. 4 for a 2 keV excitation energy. Here we focus on the single loss peak, which means loss energies up to 35 eV. To resolve the spectral contributions, we also consider, for each spectrum, the negative second derivative (whose maxima coincide with maxima in the integral spectrum). The figure shows that both spectra are resolved into features, which agree in number and energy position, apart from features D1 and D2, which are observed only on the experimental spectrum. To assign the features, we rely on previous studies[9–12] where the SiO_2 low-energy EEL spectrum was understood in terms of collective excitations and interband transitions. More specifically, and starting from the high-energy side of the spectrum, feature P at 23 eV is assigned to the bulk plasmon excitation: its energy agrees with reported values[9,13] for the bulk plasmon in amorphous SiO_2. Peaks T1–T4 are assigned to single-particle transitions and correspond to maxima in the joint density of states.[9,14] Finally, features D1 and D2 are ascribed to transitions from the VB into defect-related empty states in the band gap.[10,15] These defect states are most likely due to electron-induced rupture of Si–O bonds, leading to O desorption from the SiO_2 surface. It is worth noting that the loss intensity within the gap increases (see Fig. 3) with increasing surface sensitivity, i.e., as the primary energy decreases, which leads to locating the origin of this signal within the material surface region. A summary of the energy of the features, as derived from MC simulated and experimental spectra, is given in Table I together with literature data.

As the primary energy decreases below 2 keV, spectra change their shape, with the most pronounced evolution exhibited by experimental spectra. The evolution of the latter is given in Fig. 5, where we display spectra acquired at selected primary energies ranging from 2 keV down to 90 eV. All spectra are normalized to a common area of the zero loss peak. For the sake of clarity, they are shifted along the vertical axis. Figure 5 shows that the most noticeable change, on going from 2 keV to 90 eV, is the intensity decrease of collective bulk plasmon excitations with respect to one-electron interband transitions. The same trend is exhibited also by MC simulated spectra, as revealed in Fig. 6(a), which gives, as a function of energy, the relative weight between bulk collective excitations and single-particle interband transitions. The inset shows how the two intensities are measured on the EEL spectrum.

Concerning the observed evolution, we note that as the primary energy decreases, the surface sensitivity of experimental spectra increases, leading to a decrease in the contribution of collective bulk excitations. This interpretation is supported by Garvie *et al.*,[9] who measured the same trend on moving from bulk-to surface-sensitive loss spectra.

However, Fig. 6(a) shows the same trend also for MC simulated spectra, where surface effects are not taken into account, so that another mechanism has to be at the basis of their evolution. As mentioned above, MC simulated spectra are based on a loss function derived from optical data (i.e., with momentum transfer $q=0$), and an algorithm proposed

TABLE I. Energy band gap and EEL features (in eV) for experimental (E_0=90 eV and 2 keV) and MC simulated (E_0=2 keV) EEL spectra. Literature data (Refs. 9–13) are given for comparison.

				Ref. 8					
	REELS E_0=90 eV	REELS E_0=2 keV	MC E_0=2 keV	Bulk	Surface	Ref. 9	Ref. 10	Ref. 11	Ref. 12
Band gap	8.3	8.9	9	9.4	8.9		9.7	8.9	9.3
T1	10.6	10.7	10.5	10.6	10.6	10.3	11.6	10.7	
T2	12.9	12.6	12.3	12	12.2	12.6	12.9	12.5	
T3	14.7	14.6	14.9	14.3	14.2	13.8	15.4	14.5	
T4	17.7	18.8	18.4	18.2	17.6	17.2	18.4	17.8	
Plasmon	21.1	22.9	23	22.9		23.4		22	23.1

by Ashley[5] is used to extend the loss function to the finite momentum-transfer characteristic of electron excited spectra. It is well known that the momentum transfer associated with the inelastic collision increases when the primary energy decreases.[16] As the momentum transfer increases, the plasmon peak generally loses intensity and disperses in energy until, above a critical momentum transfer, collective excitations are completely damped by single-particle excitations. The evolution of MC simulated spectra is therefore understood in terms of a momentum-transfer change. In Fig. 6, it is clear that the increase in momentum transfer markedly affects the spectra only below 250 eV, while it hardly results in any change above this energy.

Experimental spectra, on the other hand, exhibit a continuous evolution as the primary energy decreases below 2 keV. We understand this different behavior, as compared to that of MC simulated spectra, as an indication that both surface effects and momentum-transfer related effects play a role in this case.

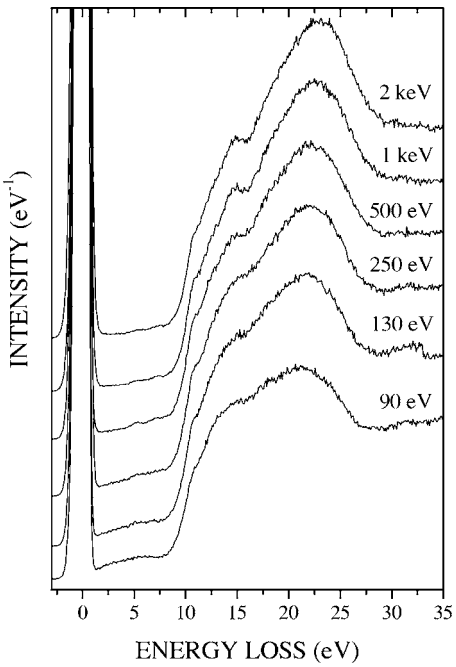

FIG. 5. Experimental EEL spectra acquired at different primary energies. All spectra are normalized to a common area of the zero loss peak. They are vertically shifted for the sake of clarity.

The evolution, as a function of the primary energy, of two additional spectral parameters is given in Fig. 6. Figure 6(b)

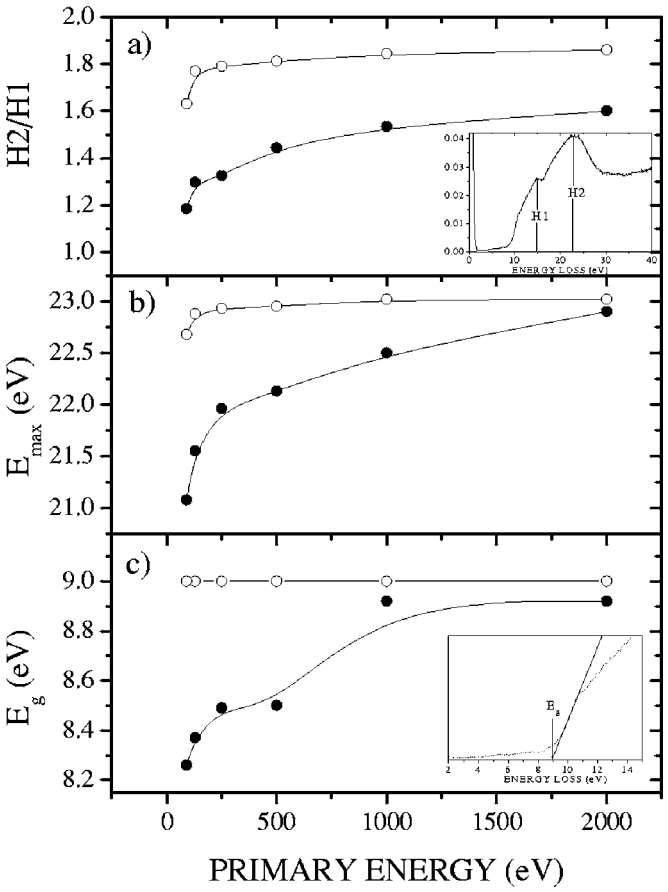

FIG. 6. Primary energy dependence of features measured on the experimental (filled circles) and on the MC simulated (open circles) EEL specta. Top panel: relative intensity of collective (H_2) and single-particle (H_1) excitations. Heights H_2 and H_1 are defined in the inset. Middle panel: energy of the maximum E_{max} of the single scattering contribution to the EEL spectrum. Bottom panel: energy band gap E_g measured by extrapolating the line corresponding to the spectrum maximum negative slope down to zero intensity, as shown in the inset.

provides the energy of the peak maximum for the single scattering contribution to the spectrum, while Fig. 6(c) gives the band-gap width. The latter is measured by linearly extrapolating to zero intensity the highest negative slope of the spectrum edge around 10 eV, as illustrated in the inset.

Figure 6(b) shows that the peak maximum energy of the single-scattering contribution decreases as the primary energy decreases. In line with Fig. 6(a), the peak shift is confined within a very narrow energy range at the low-energy end of the figure for MC simulated spectra, while it takes place over all the energy range for experimental spectra. Several factors can be responsible for this, though the main one appears to be the decrease in intensity of the bulk plasmon component within the spectrum envelope. As a result, the structure as a whole shifts to lower energy. In addition, and only for the experimental case, a small downward shift of the plasmon peak itself has to be ascribed to the band-gap narrowing at the surface revealed by Fig. 6(c) (for experimental spectra). We remember, in fact,[17] that the existence of an energy gap E_g leads to the displacement of the plasmon energy, $\hbar\omega_p$, above the energy for free electrons, $\hbar\omega_0$, according to the equation:

$$\hbar\omega_p^2 = \hbar\omega_0^2 + E_g^2. \tag{8}$$

In our case, the reduction in E_g is 0.6 eV [see Fig. 6(c)].

It has long been recognized that the SiO_2 surface is damaged by electron irradiation:[18] Si-O bonds are broken and O desorbs from the surface, thereby leading to an O depleted surface region. The process can be followed by the EEL spectrum, as shown in Fig. 7, where we display spectra acquired at increasing irradiation doses (current density ≈ 40 A/m^2). All spectra are normalized to a common area of the zero loss peak. We see that changes occur in the gap region, where the loss intensity progressively increases, and in the 15–20 eV region, where a different component develops and becomes the dominant one after a dose of 2.4×10^6 C/m^2. The difference spectrum (between spectra corresponding to the maximum and minimum irradiation doses) given at the bottom of the figure enlightens the fact that changes develop in the 2–10 and 15–20 eV regions. On the other hand, a Si spectrum given for reference on the same figure helps in understanding the origin of spectral changes. The component increasing in the 15–20 eV range is, in fact, assigned to the Si bulk plasmon loss, and signal increasing within the band gap is also ascribed to features of the elemental Si spectrum. Spectral changes thus reveal the formation of Si-Si bonds in the surface region as a consequence of O desorption.

In Fig. 8, we plot the area D, calculated from difference spectra and defined in Fig. 7, as a function of the irradiation dose on a logarithmic scale. The figure shows that a dose exists, $\approx 1.2 \times 10^4$ C/m^2, below which the material surface region is practically stable under electron irradiation. Beyond this dose, however, damage increases logarithmically with the irradiation dose. Though an investigation of the damage growth with the irradiation dose is beyond the scope of this work, we note that the observed logarithmic law is likely to derive from the transport properties of the dissociated species.[18,19] More specifically, once O is desorbed from the surface, further O desorption requires the diffusion of dissociated O from the bulk toward the surface, which limits the rate at which damage grows.

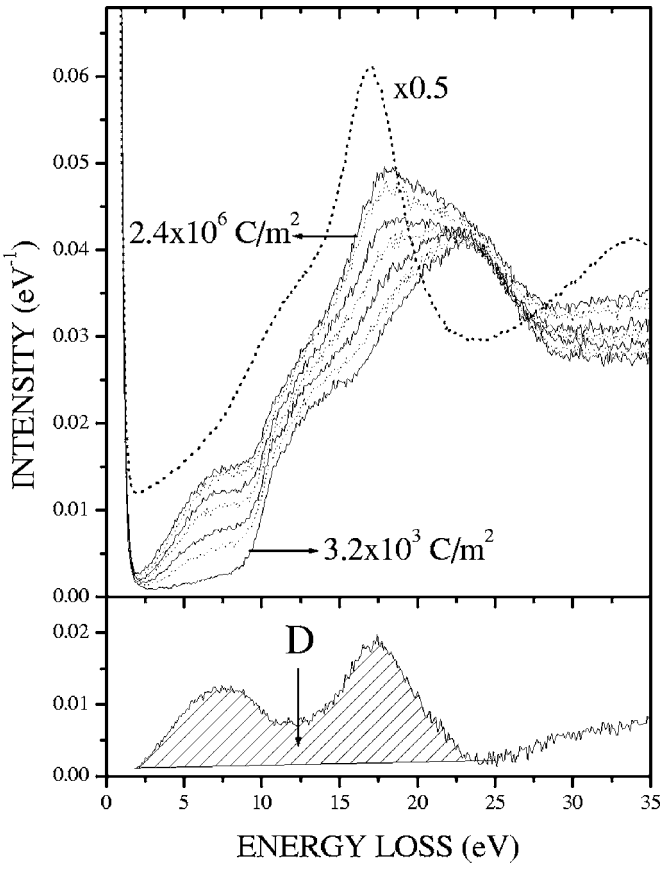

FIG. 7. Experimental EEL spectra, excited by 2 keV electrons, for different electron irradiation doses. The minimum and maximum doses are given in the figure. Spectra are normalized to a common area of the zero loss peak. The spectrum from elemental Si (whose intensity is multiplied by a factor of 0.5) is given for reference. The bottom panel shows the difference spectrum between maximum and minimum dose spectra. The striped area D is plotted in Fig. 8.

V. CONCLUSIONS

SiO_2 EEL spectra are measured for exciting energies ranging from 90 eV to 2 keV. They are compared with MC simulated EEL spectra based on an ELF derived from optical data. Quite a good agreement is obtained for 2 keV spectra, where the simulated and experimental spectra are both resolved into features, which agree in number and energy and which are assigned, on the basis of previous works on the subject, either to single-particle or to collective excitations. For both spectra, the measured energy gap agrees with previous reported data.

As the exciting energy decreases, MC simulated and experimental EEL spectra both evolve according to the same qualitative trend, which consists in an increased contribution by single-particle excitations at the expense of bulk collective excitations. Such a change is mainly responsible for the

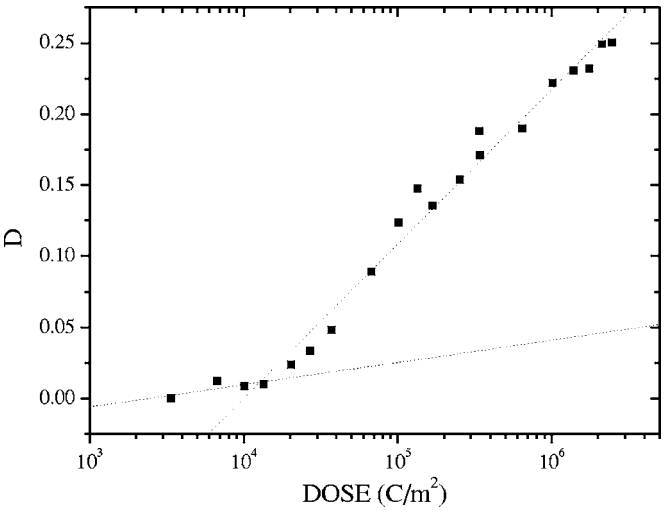

FIG. 8. Area *D*, as defined in Fig. 7, as a function of the electron dose. The experimental points are fitted by two lines showing the two regimes characterizing the development of damage as the irradiation dose increases.

observed downward shift in energy for the peak maximum of the inelastic structure associated with single scattering events. The observed evolution is assigned to the increase in momentum transfer as the primary energy decreases for MC simulated spectra, whereas, for experimental spectra, surface effects add to the momentum-transfer effect to determine the spectrum evolution.

Electron-beam-induced O desorption is revealed by experimental EEL spectra, and we briefly discuss how this material modification sets in with the irradiation dose. Care is therefore required when using EELS to characterize beam-sensitive materials such as SiO_2.

ACKNOWLEDGMENT

The work was funded by Fondo Unico per la Ricerca (Provincia Autonoma di Trento) in the frame of "Microcombi" Project.

[1] M. Dapor, Surf. Sci. **600**, 4728 (2006).
[2] M. Dapor, *Electron-Beam Interactions with Solids: Application of the Monte Carlo Method to Electron Scattering Problems*, Springer Tracts in Modern Physics (Springer-Verlag, Berlin, 2003).
[3] A. Jablonski, F. Salvat, and C. J. Powell, J. Phys. Chem. Ref. Data **33**, 409 (2004).
[4] M. Dapor, J. Appl. Phys. **79**, 8406 (1996).
[5] J. C. Ashley, J. Electron Spectrosc. Relat. Phenom. **46**, 199 (1988).
[6] B. L. Henke, E. M. Gullikson, and J. C. Davis, At. Data Nucl. Data Tables **54**, 181 (1993).
[7] U. Buechner, J. Phys. C **8**, 2781 (1975).
[8] H. Bichsel, Nucl. Instrum. Methods Phys. Res. B **52**, 136 (1990).
[9] L. A. J. Garvie, P. Rez, J. R. Alvarez, and P. R. Buseck, Solid State Commun. **106**, 303 (1998).
[10] V. M. Bermudez and V. H. Ritz, Phys. Rev. B **20**, 3446 (1979).
[11] V. J. Nithianandam and S. E. Schnatterly, Phys. Rev. B **38**, 5547 (1988).
[12] H. Ibach and J. E. Rowe, Phys. Rev. B **10**, 710 (1974).
[13] F. Yubero, S. Tougaard, E. Elizalde, and J. M. Sanz, Surf. Interface Anal. **20**, 719 (1993).
[14] L. A. J. Garvie, P. Rez, J. R. Alvarez, P. R. Buseck, A. J. Craven, and R. Brydson, Am. Mineral. **85**, 732 (2000).
[15] P. Poveda and A. Glachant, Surf. Sci. **323**, 258 (1995).
[16] Y. Ohno, Phys. Rev. B **39**, 8209 (1989).
[17] H. Raether, *Excitation of Plasmons and Interband Transitions by Electrons*, Springer Tracts in Modern Physics (Springer-Verlag, Berlin, 1982).
[18] L. Calliari and F. Marchetti, Appl. Surf. Sci. **59**, 79 (1992).
[19] G. S. Chen, C. B. Boothroyd, and C. J. Humphreys, Philos. Mag. A **78**, 491 (1998).